How to cite: *Angew. Chem. Int. Ed.* **2023,** *62,* e202218421
International Edition: doi.org/10.1002/anie.202218421
German Edition: doi.org/10.1002/ange.202218421

**Proton Conductors**

# Anhydrous Superprotonic Conductivity in the Zirconium Acid Triphosphate $ZrH_5(PO_4)_3$**

*Sacha Fop,* Riccardo Vivani, Silvia Masci, Mario Casciola, and Anna Donnadio**

**Abstract:** The development of solid-state proton conductors with high proton conductivity at low temperatures is crucial for the implementation of hydrogen-based technologies for portable and automotive applications. Here, we report on the discovery of a new crystalline metal acid triphosphate, $ZrH_5(PO_4)_3$ (ZP3), which exhibits record-high proton conductivity of $0.5–3.1\times10^{-2}$ S cm$^{-1}$ in the range 25–110 °C in anhydrous conditions. This is the highest anhydrous proton conductivity ever reported in a crystalline solid proton conductor in the range 25–110 °C. Superprotonic conductivity in ZP3 is enabled by extended defective frustrated hydrogen bond chains, where the protons are dynamically disordered over two oxygen centers. The high proton conductivity and stability in anhydrous conditions make ZP3 an excellent candidate for innovative applications in fuel cells without the need for complex water management systems, and in other energy technologies requiring fast proton transfer.

## Introduction

Solid-state proton conductors (SSPCs) are ionic conductors in which the diffusion of $H^+$ ions is responsible for charge transfer. Depending on their physicochemical characteristics and temperatures of operation, several classes of SSPCs can be identified,[1] with important applications in a range of hydrogen-based energy technologies.[2] SSPCs with minimum proton conductivity of $10^{-2}$ S cm$^{-1}$ at low temperatures ($\leq$150 °C) are in demand for the development of fuel cells and other hydrogen-related technologies for portable and automotive applications.[3] Most of the low temperature SSPCs are represented by perfluorosulfonated polymer electrolytes such as Nafion.[4] However, these polymer electrolytes have high costs and require to be hydrated (relative humidity, RH, >90 %) to maintain high ionic conductivities and prevent degradation.[5] In particular, the requirement for active humidification forces the implementation of complex water management systems, thus imposing considerable limitations on the deployment of low-temperature hydrogen technologies.[5,6] As an alternative to perfluorosulfonated polymer electrolytes, phosphoric acid-doped polybenzimidazole (PA-PBI) membranes are attracting considerable attention for electrolyte applications in fuel cells, as they can operate under anhydrous conditions.[5,7] However, the performances of PA-PBI membranes is limited by their poor mechanical properties at the high phosphoric acid-doping levels necessary to achieve desired proton conductivities.[7] Solid acids based on tetrahedral oxyanion groups like $CsH_2PO_4$ offer a further alternative to polymer electrolytes as they exhibit anhydrous proton conductivity at moderate temperatures (100–300 °C), due to a polymorphic phase transition to a highly conductive superprotonic phase characterized by highly mobile disordered protons.[8,9] Although these systems have shown good performances in fuel cells, the use of solid acids as electrolytes has been hindered by their low ionic conductivity below the phase transition, as well as the stability of the superprotonic phase which only forms in a narrow temperature range and often requires active humidification.[2e,10,11] Metal-organic frameworks (MOF) and covalent organic framework (COF) proton conductors can exhibit proton

[*] Dr. S. Fop
The Chemistry Department, University of Aberdeen
Aberdeen AB24 3UE (UK)
and
ISIS Facility, Rutherford Appleton Laboratory
Harwell OX11 0QX (UK)
E-mail: sacha.fop1@abdn.ac.uk
Prof. R. Vivani, Prof. A. Donnadio
Department of Pharmaceutical Sciences, University of Perugia
Via del Liceo 1, 06123 Perugia (Italy)
and
CEMIN—Centro di Eccellenza Materiali Innovativi Nanostrutturali per Applicazioni Chimiche, Fisiche e Biomediche, University of Perugia
Via Elce di Sotto 8, 06123 Perugia (Italy)
E-mail: anna.donnadio@unipg.it
Dr. S. Masci, Prof. M. Casciola
Department of Chemistry, Biology and Biotechnologies, University of Perugia
Via Elce di Sotto 8, 06123 Perugia (Italy)

[**] A previous version of this manuscript has been deposited on a preprint server (https://doi.org/10.26434/chemrxiv-2022-2h4g1).

conductivity under anhydrous conditions when impregnated with non-volatile acids (e.g., $H_2SO_4$ and $H_3PO_4$) or conducting media (such as organic aryl molecules like triazole and imidazole), although their conductivities and stability are often inadequate for practical applications.[12,13] The development of new SSPCs with good phase stability and high conductivity in anhydrous conditions is still an open challenge for scientists working on low and moderate temperature fuel cells and hydrogen technologies.

Here, we report on the discovery of a new zirconium acid triphosphate, $ZrH_5(PO_4)_3$ (ZP3), with record-high proton conductivity of $0.5–3.1\times10^{-2}$ S cm$^{-1}$ in the temperature range 25–110 °C in anhydrous conditions (RH ≪ 1%, $pH_2O \ll 10^{-2}$ atm). This value of anhydrous proton conductivity is unprecedent and comparable with benchmark polymer electrolytes and MOF proton conductors operating under high relative humidity. ZP3 does not exhibit any phase transition and maintains high anhydrous proton conductivity even at room temperature.

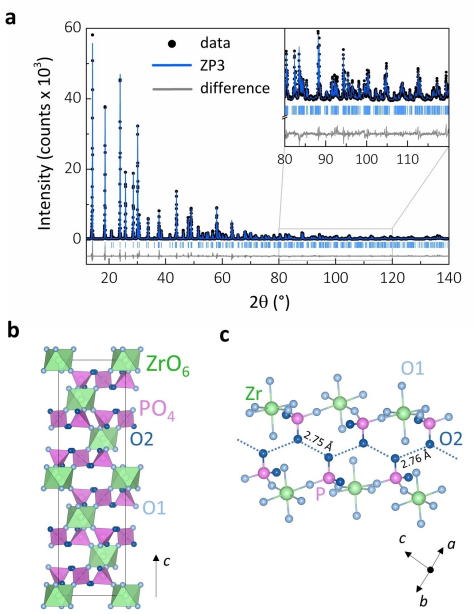


***Figure 1.*** a) Rietveld refinement fit to the powder X-ray diffraction data of ZP3. The vertical marks indicate the calculated reflection positions. b) Crystal structure of ZP3 showing the alternating layers of $ZrO_6$ octahedra and $PO_4$ tetrahedra. c) View of the hydrogen bond network connecting the non-bridging oxygen atoms of adjacent phosphate groups.

## *Results and Discussion*

Zirconium hydrogen phosphates are a class of $Zr^{IV}$ solid acids exhibiting various layered (α-$Zr(HPO_4)_2{\cdot}H_2O$, γ-$Zr(PO_4)(H_2PO_4){\cdot}2H_2O$, θ-$Zr(HPO_4)_2{\cdot}8H_2O$) and three-dimensional (τ- and τ′-$Zr(HPO_4)_2$) crystalline phases which can be formed via control of the P:Zr molar ratio and of the reaction medium and conditions.[14] ZP3 was precipitated by reacting anhydrous $ZrOCl_2$ with excess phosphoric acid (initial P:Zr molar ratio of 25) at 85 °C (see Supporting Information for further experimental details). The images from scanning electron microscopy (SEM) evidence a cubic-like morphology of the obtained ZP3 crystals (Figure S1), in contrast with the platelet-like shapes reported for layered α- and γ-zirconium phosphate.[14a,c] Inductively coupled plasma optical emission spectroscopy (ICP-OES) measurements indicated a composition of P:Zr = 2.98(5) in agreement with the nominal P:Zr ratio of 3. Results from measurements of $NH_3$ chemisorption were consistent with the presence of five acidic hydrogen atoms belonging to three phosphate groups (Table S1). Thermogravimetric (TGA) measurements until full decomposition to the pyrophosphate $ZrP_2O_7$ gave weight losses consistent with a molecular mass of 375 u (Figure S2 and Figure S3), in agreement with the nominal mass of 381 u for the chemical formula of ZP3. These results confirmed that the composition of as prepared ZP3 is $ZrH_5(PO_4)_3$.

Figure 1a shows the X-ray powder diffraction pattern of ZP3. The powder diffraction pattern could be indexed with a trigonal unit cell with lattice parameters $a = 8.27325(3)$ Å and $c = 25.5433(2)$ Å, with the most probable space group *R*-3*c* (see Supporting Information). The crystal structure of ZP3 was solved ab initio from powder X-ray diffraction data. An initial structural model was determined using the real space global optimization methods implemented in FOX with the parallel tempering algorithm,[15] and subsequently refined with the GSAS/EXPGUI software package.[16] Rietveld refinement of the obtained structural model resulted in an excellent fit to the powder diffraction data (Figure 1a), with good statistical factors and realistic atomic parameters and distances (see Table S2 for the detailed crystal data and Table S3 for selected bond lengths and angles). The structure of ZP3 is composed of a three-dimensional network of alternating layers of $PO_4$ tetrahedra and $ZrO_6$ octahedra connected via corner sharing (Figure 1b).[17] The phosphate units are constituted by two oxygen atoms shared with two adjacent Zr atoms (O1) and two non-bridging terminal oxygen atoms (O2), which are available to form hydroxyl OH groups. Adjacent non-bridging O2 atoms form a continuous network of equidistant short hydrogen bonds O2–H···O2 (2.756(2) and 2.762(2) Å) (Figure 1c). The solid-state $^{31}$P MAS NMR spectrum of ZP3 shows only one resonance at about −17 ppm, thus indicating the presence of only one type of phosphate group (Figure S4).[18] This implies that the five protons per formula unit of ZP3 are delocalized on six crystallographically equivalent non-coordinated oxygen atoms (two per phosphate group), thus resulting in a partially protonated phosphate group with average composition $PO_2(OH_{0.833})_2$. This creates a series of proton vacancies where a proton of an adjacent OH group can jump on. Such a structural network provides pathways for fast proton transport.[11b,19]

The proton conductivity of ZP3 was analyzed by AC impedance spectroscopy. The conductivity measurements were performed on a dense ZP3 pellet sample (≈93 % of the theoretical density, Figure S5) under anhydrous conditions (RH ≪ 1%, $pH_2O \ll 10^{-2}$ atm) in the temperature range 25–120 °C. Variable temperature X-ray diffraction and

differential scanning calorimetry (DSC) measurements demonstrated that ZP3 does not show any transition nor phase degradation in this temperature range (Figure S6 and Figure S7). In addition, stability tests in a range of temperatures and RH values demonstrated that the ZP3 phase is stable over a large temperature window (0–120 °C) in dry conditions (Figure S8). This is in stark contrast with the superprotonic phases of $CsH_2PO_4$ and analogous solid acids which are only stable in a narrow temperature range under dry conditions.[8–11,20] Complex impedance $Z^*$ (Nyquist) plots for ZP3 are presented in Figure 2a. The impedance spectra of ZP3 show a single straight-line response associated to the electrolyte-electrode interface, with the intercept on the real $Z'$ axis corresponding to the resistance of the polycrystalline sample. This behavior is common of materials with very high proton conductivities and large characteristic frequencies.[9,21,22]

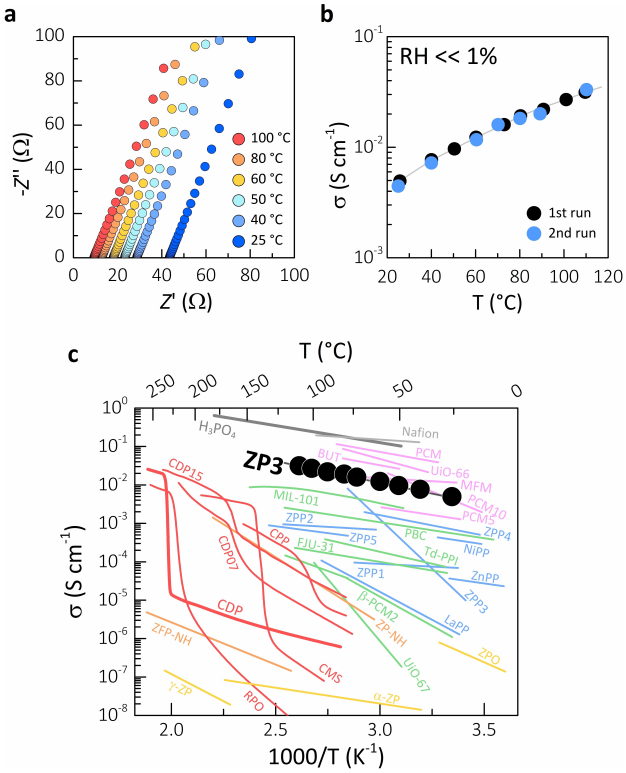


***Figure 2.*** a) Complex impedance $Z^*$ (Nyquist) plots for ZP3 collected under dry conditions (RH ≪ 1%) at various temperatures. The impedance spectra show a single straight-line response associated to the electrolyte-electrode interface. b) Proton conductivity of ZP3 measured under anhydrous conditions. Data taken over two different cooling and heating cycles is shown for comparison. c) Arrhenius plot of the anhydrous proton conductivity of ZP3 compared with other solid-state proton conducting materials. Colors represent different conductor types. Gray, benchmark polymer electrolyte Nafion at 90% RH.[26] Yellow, zirconium phosphates under anhydrous/low humidity conditions.[23] Orange, zirconium phosphates with guest $NH_4^+$ cations.[25] Red, solid acids with tetrahedral oxyanion groups showing superprotonic transitions.[2e,9,11] Blue, zirconium- and other metal-phosphonates under highly humidified conditions (RH ≥ 90%).[24] Green, proton conducting MOFs operating under anhydrous conditions.[12] Pink, proton conducting MOFs operating under highly humidified conditions (RH ≥ 90%).[21,27] The conductivity of liquid phosphoric acid $H_3PO_4$ is also included for comparison.[35] See Figure S11 for full list of compounds.

The proton conductivity of ZP3 is presented in Figure 2b. No loss of proton conductivity was observed during two cooling and heating cycles conducted over more than 120 hours, and no phase changes were detected from a diffraction pattern collected post-conductivity measurements (Figure S10), thus confirming the good stability of ZP3. Any possible contribution of $H_3PO_4$ (which could have been formed at the grain boundary during the preparation of the pellet sample) to the proton conductivity of ZP3 can be excluded or estimated to be at most ≈5% (see Supporting Information for further details). Therefore, the high ionic conductivity of ZP3 can be ascribed to fast proton transport within the bulk material. Under anhydrous conditions, ZP3 exhibits very high proton conductivity of $0.5–3.1 \times 10^{-2}$ S cm$^{-1}$ and activation energy of 0.21(1) eV between 25 and 110 °C (extracted from linear fit to the Arrhenius plot, see Supporting Information), which are in the range of superprotonic conductivity.[9,11,21] Zirconium phosphates like α-$Zr(HPO_4)_2{\cdot}H_2O$, γ-$Zr(PO_4)(H_2PO_4){\cdot}2H_2O$, τ-$Zr(HPO_4)_2$ and $ZrP_2O_7$ are generally poor proton conductors with conductivities in the range $10^{-8}$–$10^{-7}$ S cm$^{-1}$ under anhydrous conditions, rising to $10^{-6}$–$10^{-5}$ S cm$^{-1}$ at RH > 90%.[14e,23] Zirconium phosphonates have proton conductivities of $10^{-4}$–$10^{-2}$ S cm$^{-1}$ at RH > 90%, although these values dramatically drop to $10^{-6}$–$10^{-5}$ S cm$^{-1}$ when RH is reduced.[24] The high anhydrous superprotonic conductivity of ZP3 is a unique and unprecedented characteristic among zirconium phosphate and phosphonate materials.

As shown in the Arrhenius plots in Figure 2c (see also Figure S11), ZP3 outperforms the conductivities of traditional oxyanion solid acids by 2 to 8 orders of magnitude in the temperature range 25–110 °C (see also Table S4). The conductivity of ZP3 far exceeds the anhydrous proton conductivity values recently reported for zirconium phosphate crystals containing guest $NH_4^+$ cations (in the range $10^{-5}$–$10^{-3}$ S cm$^{-1}$ between 90 and 230 °C)[25] and of many anhydrous MOF proton conductors.[12] ZP3 exhibits record-high conductivity when compared to oxyanion solid acid conductors, and, to the best of our knowledge, the highest anhydrous proton conductivity ever reported in a crystalline solid proton conductor in the range 25–110 °C. The anhydrous proton conductivity of ZP3 is competitive with the conductivities of benchmark polymer electrolyte Nafion[26] and of the best-performing MOF proton conductors operating under highly humidified conditions.[21,27] Polymer electrolytes require active humidification to prevent dehydration and maintain desirable conductivity levels.[5] Similarly, hydrated MOF proton conductors necessitate high RH values or post-synthetic modifications in order to introduce protonic defects and/or vehicular species enabling adequate levels of proton conduction.[12,21,27] In contrast, ZP3 exhibits superprotonic conductivity due to fast transport of native protonic defects under anhydrous conditions. The anhydrous superprotonic conductivity and good stability make ZP3 particularly interesting for applications in solid-state electrochemical hydrogen technologies

operating at low/intermediate temperatures and without the need of humidifcation.

To investigate the ionic conduction mechanism, the energy landscape for a test $H^+$ was calculated by the bond-valence sum energy (BVSE) method with the software *soft*BV,[28] using the structural model from Rietveld refinement as input. This method has successfully been employed for the determination of the ionic migration pathways and mechanism in several types of solid ionic conductors,[29] as well as for the identification of accurate lowest-energy equilibrium proton positions in solid oxide proton conductors.[30] Two lowest energy (0.0 eV absolute BVSE minimum) equilibrium proton positions were identified at Wyckoff position 36*f*, around the non-bridging O2 atoms of the $PO_4$ tetrahedra (Figure 3a and Figure S12a). H1 is at ($\approx$0.01, 0.5, $\approx$0.99) and H2 at ($\approx$0.98, $\approx$0.79, $\approx$0.74). Protons are bistable on two off-centre sites between two O2 atoms which compete as hydrogen bond donor and acceptor due to the short –O2···O2– distance (Figure S12a).[25b,31,32] The BVSE analysis shows low energy (<0.19 eV) connecting isosurfaces across the H1 and H2 positions, indicating 1-dimensional conduction pathways along the hydrogen bond network (Figure 3a, compare with Figure 1c).

Proton migration follows a Grotthuss-like mechanism composed by the rotation ($\approx$121°) of a proton from the position H1 to H2 (or vice versa) and hopping onto an adjacent O2 atom (Figure 3b). The H1–H2 rotation has the higher activation barrier (*S1*) of 0.182 eV, a value which agrees well with the experimental activation energy. Proton hopping between two adjacent O2 atoms (*S2*) has an almost negligible activation energy (0.007 eV). Proton transfer in ZP3 is fast thanks to the favorable hydrogen bond network, where the protons are dynamically disordered over two oxygen centers (with essentially equivalent –O2···O2– distances) in a symmetric double potential well, and can easily interchange their donor and acceptor sites along hydrogen-bonded chains (Figure S12b).[1a,32] The configuration of the hydrogen-bonded chains and the phosphate composition $PO_2(OH_{0.833})_2$ strongly suggest a high hydrogen bond network frustration (an indirect indication for hydrogen bond network frustration is the high hygroscopicity of ZP3, because hydration is one way to reduce frustration).[33] The hydrogen bond network is frustrated when there is an imbalance of potential proton donors and acceptors. Hydrogen bond frustration plays a fundamental role in defining the proton conducting properties of phosphoric acid $H_3PO_4$ (the compound with the highest intrinsic proton conductivity in the liquid state) and phosphorous oxyacids in general.[32] For example, while $H_3PO_4$ [$P(OH_{0.75})_4$] has a lower concentration of proton defects than phosphinic acid $H_3PO_2$ [$PH_2(OH_{0.5})_2$)], the proton conductivity of phosphoric acid is much higher due to the presence of high hydrogen bond network frustration (three O–H donors and only one non-protonated oxygen) and extended polarized hydrogen-bonded chains.[34,35] Hydrogen bond network frustration induces cooperativity of proton transfer events and enables fast depolarization of polarized hydrogen bond chains, thus enabling high proton conductivity.[34] Similarly to $H_3PO_4$, ZP3 presents an extended network of defective hydrogen-bonded chains where protons are frustrated running through the entire crystal structure and enabling long-range correlated fast proton motion (Figure 3c and Figure S13).[34] These findings are of strong fundamental relevance as they evidence a conduction mechanism never seen before in a solid acid. High proton conductivity in traditional solid acids based on tetrahedral oxyanion groups is generally due to a phase transition from an ordered low conducting phase (< $10^{-6}$ S cm$^{-1}$) to a high temperature (>150 °C) disordered superprotonic cubic phase.[9–11] For example, the ordered phase of $CsH_2PO_4$ has low hydrogen bond network frustration (two hydrogen bond donor groups and two hydrogen bond acceptors),[31] thus resulting in limited proton conductivity below the phase transition. Instead, our results demonstrate that superprotonic conductivity in ZP3 is enabled even at room temperature thanks to the presence of defective hydrogen-bonded chains where protons are frustrated and require minimal activation energy for hopping. Further neutron scattering experiments will be necessary to confirm the mechanism of fast proton conduction.

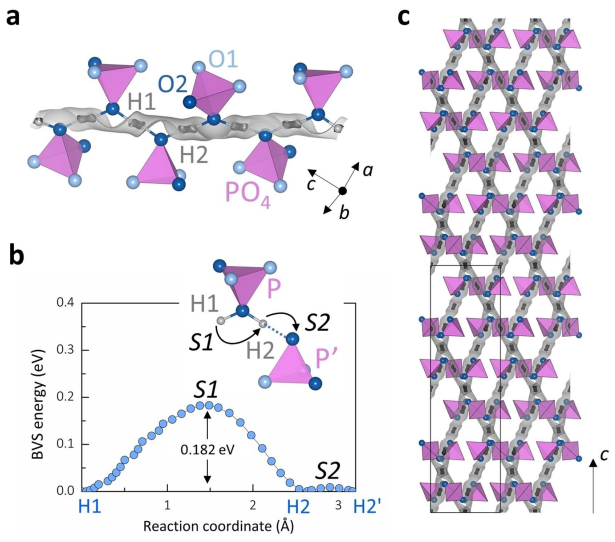


***Figure 3.*** a) BVSE map for a test $H^+$ (isosurface levels are drawn at <0.19 eV) showing 1-dimensional connectivity and indicating proton conduction pathways along the terminal O2 oxygen atoms of adjacent phosphate groups. Darker isosurface levels are drawn at 0.0 eV and correspond to the equilibrium proton positions H1 and H2. b) BVSE barrier and schematic of the proton diffusion mechanism, which is composed by rotation from H1 to H2 (or vice versa) (*S1*) and hopping onto an adjacent terminal O2 atom (*S2*). c) Proton migration network within the ZP3 structure.

## Conclusion

In summary, we have synthesized and characterized a new zirconium acid triphosphate, $ZrH_5(PO_4)_3$ (ZP3), exhibiting remarkable superprotonic conductivity under anhydrous conditions. The fast proton transport is due to the particular configuration and spatial orientation of extended hydrogen-bonding chains where protons can readily diffuse. ZP3 is the first example of a new class of SSPCs for electrolyte

applications in fuel cells without the need of humidification, thus greatly simplifying the fuel cell system, at a temperature range useful for portable applications and transportation. It is also worth noting that the superprotonic conductivity at room temperature of ZP3 is at par with some of the best solid-state lithium-ion conductors, implying that ZP3 could also be employed for the development of innovative full solid-state proton batteries,[36] and other energy or catalytic technologies requiring fast proton transfer.

## Acknowledgements

S.F. gratefully acknowledges the Ramsay Memorial Trust and the University of Aberdeen's School of Natural and Computing Sciences for the provision of a Ramsay Memorial Fellowship. This paper benefited from the insights of Professor Giulio Alberti who was a pioneer and one of the most authoritative scientists of the chemistry of $M^{IV}$ phosphates and phosphonates.

## Conflict of Interest

The authors declare no conflict of interest.

## Data Availability Statement

The data that support the findings of this study are available from the corresponding author upon reasonable request.

**Keywords:** Zirconium Phosphates · Conducting Materials · Fuel Cells · Proton Conductivity · Solid Acids

[1] a) K. D. Kreuer, *Chem. Mater.* **1996**, *8*, 610–641; b) T. Norby, *Solid State Ionics* **1999**, *125*, 1–11.

[2] a) K. D. Kreuer, *Chem. Mater.* **2014**, *26*, 361–380; b) C. Duan, J. Tong, M. Shang, S. Nikodemski, M. Sanders, S. Ricote, A. Almansoori, R. O'Hayre, *Science* **2015**, *349*, 1321–1326; c) C. Duan, R. Kee, H. Zhu, N. Sullivan, L. Zhu, L. Bian, D. Jennings, R. O'Hayre, *Nat. Energy* **2019**, *4*, 230–240; d) S. Fop, *J. Mater. Chem. A* **2021**, *9*, 18836–18856; e) S. M. Haile, D. A. Boysen, C. R. I. Chisholm, R. B. Merle, *Nature* **2001**, *410*, 910–913; f) Y. Zhou, J. Yang, H. Su, J. Zeng, S. P. Jiang, W. A. Goddard, *J. Am. Chem. Soc.* **2014**, *136*, 4954–4964; g) S. Li, Q. Xu, *Energy Environ. Sci.* **2013**, *6*, 1656–1683; h) P. Ramaswamy, N. E. Wong, G. K. H. Shimizu, *Chem. Soc. Rev.* **2014**, *43*, 5913–5932; i) S. C. Pal, M. C. Das, *Adv. Funct. Mater.* **2021**, *31*, 2101584; j) W. Xue, C. D. Sewell, Q. Zhou, Z. Lin, *Angew. Chem. Int. Ed.* **2022**, *61*, e202206512; *Angew. Chem.* **2022**, *134*, e202206512.

[3] a) O. Gröger, H. A. Gasteiger, J. P. Suchsland, *J. Electrochem. Soc.* **2015**, *162*, A2605–A2622; b) Z. P. Cano, D. Banham, S. Ye, A. Hintennach, J. Lu, M. Fowler, Z. Chen, *Nat. Energy* **2018**, *3*, 279–289; c) B. G. Pollet, S. S. Kocha, I. Staffell, *Curr. Opin. Electrochem.* **2019**, *16*, 90–95; d) M. A. Chetouane, B. Negrou, M. Becherif, N. Settou, A. Bouferrouk, M. Ramadan, *Energy Technol.* **2021**, *9*, 2100242; e) K. Jiao, J. Xuan, Q. Du, Z. Bao, B. Xie, B. Wang, Y. Zhao, L. Fan, H. Wang, Z. Hou, S. Huo, N. P. Brandon, Y. Yin, M. D. Guiver, *Nature* **2021**, *595*, 361–369.

[4] a) Z. Yang, R. G. Rajendran, *Angew. Chem. Int. Ed.* **2005**, *44*, 564–567; *Angew. Chem.* **2005**, *117*, 570–573; b) R. Kannan, B. Kakade, V. Pillai, *Angew. Chem. Int. Ed.* **2008**, *47*, 2653–2656; *Angew. Chem.* **2008**, *120*, 2693–2696; c) J. Song, O. H. Han, S. Han, *Angew. Chem. Int. Ed.* **2015**, *54*, 3615–3620; *Angew. Chem.* **2015**, *127*, 3686–3691.

[5] a) Q. Li, R. He, J. O. Jensen, N. J. Bjerrum, *Chem. Mater.* **2003**, *15*, 4896–4915; b) J. A. Asensio, E. M. Sánchez, P. Gómez-Romero, *Chem. Soc. Rev.* **2010**, *39*, 3210–3239; c) R. Singh, A. S. Oberoi, T. Singh, *Int. J. Energy Res.* **2022**, *46*, 3810–3842.

[6] B. C. Steele, A. Heinzel, *Nature* **2001**, *414*, 345–352.

[7] a) J. S. Wainright, J.-T. Wang, D. Weng, R. F. Savinell, M. Litt, *J. Electrochem. Soc.* **1995**, *142*, L121; b) L. Qingfeng, H. Hjuler, N. Bjerrum, *J. Appl. Electrochem.* **2001**, *31*, 773–779; c) Q. Li, R. He, J. O. Jensen, N. Bjerrum, *Fuel Cells* **2004**, *4*, 147–159; d) R. He, Q. Li, A. Bach, J. O. Jensen, N. J. Bjerrum, *J. Membr. Sci.* **2006**, *277*, 38–45.

[8] A. I. Baranov, *Crystallogr. Rep.* **2003**, *48*, 1012–1037.

[9] A. M. Haile, C. R. I. Chisholm, K. Sasaki, D. A. Boysen, T. Uda, *Faraday Discuss.* **2007**, *134*, 17–39.

[10] D. A. Boysen, T. Uda, R. I. C. Calum, S. M. Haile, *Science* **2004**, *303*, 68–70.

[11] a) L. S. Wang, S. V. Patel, S. S. Sanghvi, Y. Hu, S. M. Haile, *J. Am. Chem. Soc.* **2020**, *142*, 19992–20001; b) L. S. Wang, S. V. Patel, E. Truong, Y. Hu, S. M. Haile, *Chem. Mater.* **2022**, *34*, 1809–1820.

[12] a) J. A. Hurd, R. Vaidhyanathan, V. Thangadurai, C. I. Ratcliffe, I. L. Moudrakovski, G. K. H. Shimizu, *Nat. Chem.* **2009**, *1*, 705–710; b) V. G. Ponomareva, K. A. Kovalenko, A. P. Chupakhin, D. N. Dybtsev, E. S. Shutova, V. P. Fedin, *J. Am. Chem. Soc.* **2012**, *134*, 15640–15643; c) M. Yoon, K. Suh, S. Natarajan, K. Kim, *Angew. Chem. Int. Ed.* **2013**, *52*, 2688–2700; *Angew. Chem.* **2013**, *125*, 2752–2764; d) Y. Ye, L. Zhang, Q. Peng, G. Wang, Y. Shen, Z. Li, L. Wang, X. Ma, Q. Chen, Z. Zhang, S. Xiang, *J. Am. Chem. Soc.* **2015**, *137*, 913–918; e) S. Liu, Z. Yue, Y. Liu, *Dalton Trans.* **2015**, *44*, 12976–12980; f) Y. Ye, X. Wu, Z. Yao, L. Wu, Z. Cai, L. Wang, X. Ma, Q. Chen, Z. Zhang, S. Xiang, *J. Mater. Chem. A* **2016**, *4*, 4062–4070.

[13] a) D. Lim, H. Kitagawa, *Chem. Rev.* **2020**, *120*, 8416–8467; b) Y. Ye, L. Gong, S. Xiang, Z. Zhang, B. Chen, *Adv. Mater.* **2020**, *32*, 1907090; c) D. Lim, H. Kitagawa, *Chem. Soc. Rev.* **2021**, *50*, 6349–6368.

[14] a) D. Capitani, M. Casciola, A. Donnadio, R. Vivani, *Inorg. Chem.* **2010**, *49*, 9409–9415; b) Y. Cheng, X. Wang, S. Jaenicke, G. Chuah, *ChemSusChem* **2017**, *10*, 3235–3242; c) Y. Cheng, X. Xiadong Wang, S. Jaenicke, G. Chuah, *Inorg. Chem.* **2018**, *57*, 4370–4378; d) T. Kijima, *Bull. Chem. Soc. Jpn.* **1982**, *55*, 3031–3032; e) A. M. Krogh Andersen, P. Norby, J. C. Hanson, T. Vogt, *Inorg. Chem.* **1998**, *37*, 876–881; f) M. Pica, R. Vivani, A. Donnadio, E. Troni, S. Fop, M. Casciola, *Inorg. Chem.* **2015**, *54*, 9146–9153.

[15] V. Favre-Nicolin, R. Cerný, *J. Appl. Crystallogr.* **2002**, *35*, 734–743.

[16] a) A. C. Larson, R. B. Von Dreele, Technical Report No. LAUR86-748, Los Alamos National Laboratory **2004**; b) B. H. Toby, *J. Appl. Crystallogr.* **2001**, *34*, 210–213.

[17] Deposition Number 2209747 contains the supplementary crystallographic data for this paper. These data are provided free of charge by the joint Cambridge Crystallographic Data Centre and Fachinformationszentrum Karlsruhe Access Structures service.

[18] N. J. Clayden, *J. Chem. Soc. Dalton Trans.* **1987**, 1877–1881.

[19] a) M. Sadakiyo, T. Yamada, K. Honda, H. Matsui, H. Kitagawa, *J. Am. Chem. Soc.* **2014**, *136*, 7701–7707; b) M.

Sadakiyo, T. Yamada, H. Kitagawa, *J. Am. Chem. Soc.* **2014**, *136*, 13166–13169; c) Y. Wei, X. Hu, Z. Han, X. Dong, S. Zang, T. C. W. Mak, *J. Am. Chem. Soc.* **2017**, *139*, 3505–3512.

[20] S. M. Haile, H. Liu, R. A. Secco, *Chem. Mater.* **2003**, *15*, 727–736.

[21] a) S. S. Nagarkar, S. M. Unni, A. Sharma, S. Kurungot, S. K. Ghosh, *Angew. Chem. Int. Ed.* **2014**, *53*, 2638–2642; *Angew. Chem.* **2014**, *126*, 2676–2680; b) W. J. Phang, H. Jo, W. R. Lee, J. H. Song, K. Yoo, B. Kim, C. S. Hong, *Angew. Chem. Int. Ed.* **2015**, *54*, 5142–5146; *Angew. Chem.* **2015**, *127*, 5231–5235; c) H. S. Sasmal, H. B. Aiyappa, S. N. Bhange, S. Karak, A. Halder, S. Kurungot, R. Banerjee, *Angew. Chem. Int. Ed.* **2018**, *57*, 10894–10898; *Angew. Chem.* **2018**, *130*, 11060–11064; d) A. Sharma, J. Lim, S. Jeong, S. Won, J. Seong, S. Lee, Y. S. Kim, S. B. Baek, M. S. Lah, *Angew. Chem. Int. Ed.* **2021**, *60*, 14334–14338; *Angew. Chem.* **2021**, *133*, 14455–14459.

[22] a) I. M. Hodge, M. D. Ingram, A. R. West, *J. Electroanal. Chem.* **1976**, *74*, 125–143; b) J. T. S. Irvine, D. C. Sinclair, A. R. West, *Adv. Mater.* **1990**, *2*, 132–138.

[23] a) G. Alberti, M. Casciola in *Proton Conductors: Solids, Membranes and Gels - Materials and Devices* (Ed.: P. Colomban), Cambridge University Press, **1992**, pp. 238–253; b) M. Casciola, D. Bianchi, *Solid State Ionics* **1985**, *17*, 287–293; c) G. Alberti, M. G. Bernasconi, M. Casciola, *React. Polym.* **1989**, *11*, 245–252; d) G. Alberti, M. Casciola, S. Cavalaglio, R. Vivani, *Solid State Ionics* **1999**, *125*, 91–97.

[24] a) G. Alberti, M. Casciola, R. Palombari, A. Peraio, *Solid State Ionics* **1992**, *58*, 339–344; b) G. Alberti, L. Boccali, M. Casciola, L. Massinelli, E. Montoneri, *Solid State Ionics* **1996**, *84*, 97–104; c) F. Costantino, A. Donnadio, M. Casciola, *Inorg. Chem.* **2012**, *51*, 6992–7000; d) M. Taddei, A. Donnadio, F. Costantino, R. Vivani, M. Casciola, *Inorg. Chem.* **2013**, *52*, 12131–12139; e) Z. Hassanzadeh Fard, N. E. Wong, C. D. Malliakas, P. Ramaswamy, J. M. Taylor, K. Otsubo, G. K. H. Shimizu, *Chem. Mater.* **2018**, *30*, 314–318; f) J. M. Taylor, T. Komatsu, S. Dekura, K. Otsubo, M. Takata, H. Kitagawa, *J. Am. Chem. Soc.* **2015**, *137*, 11498–11506; g) A. Donnadio, M. Nocchetti, F. Costantino, M. Taddei, M. Casciola, F. da Silva Lisboa, R. Vivani, *Inorg. Chem.* **2014**, *53*, 13220–13226.

[25] a) D. Gui, T. Zheng, J. Xie, Y. Cai, Y. Wang, L. Chen, J. Diwu, Z. Chai, S. Wang, *Inorg. Chem.* **2016**, *55*, 12508–12511; b) D. Gui, X. Dai, Z. Tao, T. Zheng, X. Wang, M. A. Silver, J. Shu, L. Chen, Y. Wang, T. Zhang, J. Xie, L. Zou, Y. Xia, J. Zhang, J. Zhang, L. Zhao, J. Diwu, R. Zhou, Z. Chai, S. Wang, *J. Am. Chem. Soc.* **2018**, *140*, 6146–6155; c) D. Gui, J. Zhang, X. Wang, C. Wang, Q. Wang, Y. Zhang, H. Li, S. Wang, *Dalton Trans.* **2022**, *51*, 8182–8185.

[26] M. Casciola, A. Donnadio, P. Sassi, *J. Power Sources* **2013**, *235*, 129–134.

[27] a) S. Kim, B. Joarder, J. A. Hurd, J. Zhang, K. W. Dawson, B. S. Gelfand, N. E. Wong, G. K. H. Shimizu, *J. Am. Chem. Soc.* **2018**, *140*, 1077–1082; b) J. M. Taylor, K. W. Dawson, G. K. H. Shimizu, *J. Am. Chem. Soc.* **2013**, *135*, 1193–1196; c) P. Ramaswamy, N. E. Wong, B. S. Gelfand, G. K. H. Shimizu, *J. Am. Chem. Soc.* **2015**, *137*, 7640–7643; d) J. Chen, Q. Mei, Y. Chen, C. Marsh, B. An, X. Han, I. P. Silverwood, M. Li, Y. Cheng, M. He, X. Chen, W. Li, M. Kippax-Jones, D. Crawshaw, M. D. Frogley, S. J. Day, V. García-Sakai, P. Manuel, A. Ramirez-Cuesta, S. Yang, M. Schröder, *J. Am. Chem. Soc.* **2022**, *144*, 11969–11974; e) F. Yang, G. Xu, Y. Dou, B. Wang, H. Zhang, H. Wu, W. Zhou, J. Li, B. Chen, *Nat. Energy* **2017**, *2*, 877–883; f) S. Wang, M. Wahiduzzaman, L. Davis, A. Tissot, W. Shepard, J. Marrot, C. Martineau-Corcos, D. Hamdane, G. Maurin, S. Devautour-Vinot, C. Serre, *Nat. Commun.* **2018**, *9*, 4937; g) Q. Zhai, C. Mao, X. Zhao, Q. Lin, F. Bu, X. Chen, X. Bu, P. Feng, *Angew. Chem. Int. Ed.* **2015**, *54*, 7886–7890; *Angew. Chem.* **2015**, *127*, 7997–8001; h) D. D. Borges, S. Devautour-Vinot, H. Jobic, J. Ollivier, F. Nouar, R. Semino, T. Devic, C. Serre, F. Paesani, G. Maurin, *Angew. Chem. Int. Ed.* **2016**, *55*, 3919–3924; *Angew. Chem.* **2016**, *128*, 3987–3992; i) S. M. Elahi, S. Chand, W. Deng, A. Pal, M. C. Das, *Angew. Chem. Int. Ed.* **2018**, *57*, 6662–6666; *Angew. Chem.* **2018**, *130*, 6772–6776.

[28] a) H. Chen, L. L. Wong, S. Adams, *Acta Crystallogr. Sect. B* **2019**, *75*, 18–33; b) L. L. Wong, K. C. Phuah, R. Dai, H. Chen, W. S. Chew, S. Adams, *Chem. Mater.* **2021**, *33*, 625–641.

[29] a) W. Zhang, K. Fujii, E. Niwa, M. Hagihala, T. Kamiyama, M. Yashima, *Nat. Commun.* **2020**, *11*, 1224; b) K. Wang, Q. Ren, Z. Gu, C. Duan, J. Wang, F. Zhu, Y. Fu, J. Hao, J. Zhu, L. He, C. Wang, Y. Lu, J. Ma, C. Ma, *Nat. Commun.* **2021**, *12*, 4410; c) A. Banik, W. G. Zeier, H. M. Wilkening, *J. Am. Chem. Soc.* **2022**, *144*, 1795–1812; d) M. A. Plass, S. Bette, R. E. Dinnebier, B. V. Lotsch, *Chem. Mater.* **2022**, *34*, 3227–3235.

[30] a) T. Murakami, J. R. Hester, M. Yashima, *J. Am. Chem. Soc.* **2020**, *142*, 11653–11657; b) S. Fop, J. A. Dawson, A. D. Fortes, C. Ritter, A. C. McLaughlin, *Chem. Mater.* **2021**, *33*, 4651–4660; c) S. Fop, J. A. Dawson, D. N. Tawse, M. G. Skellern, J. M. S. Skakle, A. C. McLaughlin, *Chem. Mater.* **2022**, *34*, 8190–8197.

[31] G. Kim, J. M. Griffin, F. Blanc, S. M. Haile, C. P. Grey, *J. Am. Chem. Soc.* **2015**, *137*, 3867–3876.

[32] A. Katrusiak, *Phys. Rev. B* **1993**, *48*, 2992–3002.

[33] J.-P. Melchior, G. Majer, K. D. Kreuer, *Phys. Chem. Chem. Phys.* **2017**, *19*, 601–612.

[34] a) L. Vilčiauskas, M. E. Tuckerman, G. Bester, S. J. Paddison, K. D. Kreuer, *Nat. Chem.* **2012**, *4*, 461–466; b) R. A. Krueger, L. Vilčiauskas, J.-P. Melchior, G. Bester, K. D. Kreuer, *J. Phys. Chem. B* **2015**, *119*, 15866–15875.

[35] L. Vilčiauskas, C. C. De Araujo, K. D. Kreuer, *Solid State Ionics* **2012**, *212*, 6–9.

[36] a) Y. Xu, X. Wu, H. Jiang, L. Tang, K. Y. Koga, C. Fang, J. Lu, X. Ji, *Angew. Chem. Int. Ed.* **2020**, *59*, 22007–22011; *Angew. Chem.* **2020**, *132*, 22191–22195; b) F. Yue, Z. Tie, S. Deng, S. Wang, M. Yang, Z. Niu, *Angew. Chem. Int. Ed.* **2021**, *60*, 13882–13886; *Angew. Chem.* **2021**, *133*, 14001–14005; c) Z. Zhu, W. Wang, Y. Yin, Y. Meng, Z. Liu, T. Jiang, Q. Peng, J. Sun, W. Chen, *J. Am. Chem. Soc.* **2021**, *143*, 20302–20308.

Manuscript received: December 13, 2022
Accepted manuscript online: March 1, 2023
Version of record online: March 23, 2023